


Letter

Effect of Thiol Molecular Structure on the Sensitivity of Gold Nanoparticle-Based Chemiresistors toward Carbonyl Compounds

Zhenzhen Xie ^{1,†}, Mandapati V. Ramakrishnam Raju ^{2,†}, Prasadanie K. Adhichetty ³,
Xiao-An Fu ¹  and Michael H. Nantz ^{3,*} 

¹ Department of Chemical Engineering, University of Louisville, Louisville, KY 40208, USA; zhenzhen.xie@louisville.edu (Z.X.); xiaoan.fu@louisville.edu (X.-A.F.)

² Department of Chemistry, University of Minnesota, Minneapolis, MN 55455, USA; smandapa@umn.edu

³ Department of Chemistry, University of Louisville, Louisville, KY 40208, USA; prasadi.adhichetty@louisville.edu

* Correspondence: michael.nantz@louisville.edu

† These authors contributed equally.

Received: 2 November 2020; Accepted: 4 December 2020; Published: 8 December 2020



Abstract: Increasing both the sensitivity and selectivity of thiol-functionalized gold nanoparticle chemiresistors remains a challenging issue in the quest to develop real-time gas sensors. The effects of thiol molecular structure on such sensor properties are not well understood. This study investigates the effects of steric as well as electronic effects in a panel of substituted thiol-urea compounds on the sensing properties of thiolate monolayer-protected gold nanoparticle chemiresistors. Three series of urea-substituted thiols with different peripheral end groups were synthesized for the study and used to prepare gold nanoparticle-based chemiresistors. The responses of the prepared sensors to trace volatile analytes were significantly affected by the urea functional motifs. The largest response for sensing acetone among the three series was observed for the thiol-urea sensor featuring a tert-butyl end group. Furthermore, the ligands fitted with N, N'-dialkyl urea moieties exhibit a much larger response to carbonyl analytes than the more acidic urea series containing N-alkoxy-N'-alkyl urea and N, N'-dialkoxy urea groups with the same peripheral end groups. The results show that the peripheral molecular structure of thiolate-coated gold nanoparticles plays a critical role in sensing target analytes.

Keywords: molecular selectivity; carbonyl sensing; urea; alkoxy urea; bis(alkoxy) urea

1. Introduction

Monolayer protected gold clusters (MPCs) have attracted wide attention due to their unique electronic, electrochemical and biochemical properties [1–5] as well as their broad applications in materials science and biomedical diagnostics, where MPCs have been used as sensors [6–8], catalysts [9,10], biological imaging agents [11], and in studies on optics [12]. Many materials, including metal oxide nanoparticles and nanowires [13–17] and composites [18–20], semiconductors [21], carbon nanotubes [22,23], and polymer nanofibers [24,25], have been studied for the detection of a variety of volatile organic compounds (VOCs). However, these materials have encountered several challenges, including poor sensitivity and selectivity, lack of reproducibility, and large power consumption. Continued development of MPCs fitted with novel surface functionality has the potential to overcome these problems. The important characteristics of MPCs include operation at ambient temperature, variability in functional thiolate ligands, and the radial nature of the ligand monolayer arising from the faceted surface of the metal core [3,26,27].

Since Wohltjen and Snow reported the first chemiresistors of thiol-functionalized gold nanoparticles (AuNPs) for VOC detection [6], many researchers have investigated AuNP-based gas sensors for detecting various VOCs [28–32]. Unfortunately, high sensitivity and selectivity of AuNP chemiresistors toward sensing target analytes such as formaldehyde and acetone have not been demonstrated [4]. Furthermore, the effect of thiol molecular structure on the sensitivity and selectivity of thiol-functionalized AuNPs sensors has not been widely studied due to the limited availability of custom thiols. Most of the published AuNP-based gas sensors were prepared using commercial thiol-functionalized AuNPs [28–32].

The objective of this work is to identify new AuNP ligands that can significantly increase both sensitivity and selectivity for sensing carbonyl compounds by forming strong hydrogen-bonds with the carbonyl group of target analytes, such as formaldehyde, acetaldehyde and acetone. Formaldehyde, acetaldehyde and acetone are ubiquitous in environmental air. Chronic exposure to high concentrations of formaldehyde, acetaldehyde and acrolein can cause lung cancer and cardiovascular disease [33]. These aldehydes in the atmosphere are continuously monitored by the United States Environmental Protection Agency (EPA) under the National Air Toxics Assessment (NATA) program [34]. We sought to promote hydrogen-bond formation by incorporation of urea moieties on the surfaces of AuNPs for the detection of these carbonyl compounds in air. Hydrogen bonding has been used previously to promote crystal structures of adducts between urea and acetone derivatives [35]. We recently disclosed a synthesis of the urea-substituted thiol ligand 1-(tert-butyl)-3-((11-mercapto-undecyl)oxy)urea and its use in a AuNP-based sensor for detecting acetone in air [36]. We now seek to study the effects of peripheral end groups of this class of thiolate ligand to better understand how modulation of steric and electronic interactions influences chemiresistor sensitivity and selectivity. Steric interactions between the peripheral end groups can have significant effects on surface packing and thus on the stability and electronic behavior of AuNPs [37]. In the present work, three series of thiol-urea ligands were synthesized and then tested as sensing materials by incorporation onto AuNP chemiresistors. We report herein the results of acetone sensing studies and trends observed on varying the urea structure as well as peripheral groups.

2. Materials and Methods

2.1. Materials

11-Bromo-1-undecene, thioacetic acid, and tert-butyl isocyanate were purchased from Sigma-Aldrich (St. Louis, MO, USA). N-Alkoxyphthalimide 1 (Scheme 1) was synthesized according to a published procedure [38]. Amine 4 (Scheme 2) and 1-(tert-butyl)-3-((11-mercapto-undecyl)-oxy)urea were prepared according to literature methods [39,40]. Hydrogen tetrachloroaurate (HAuCl_4) and tetraoctylammonium bromide (TOAB) were obtained from Sigma-Aldrich. Sodium borohydride was purchased from Fluka (Buchs, Switzerland). Tedlar bags were purchased from Supelco (Bellefonte, PA, USA). Synthetic air with less than 4 ppm of moisture was obtained from a local gas supply company. Deionized water was used throughout this work.

Tetrahydrofuran (THF) was dried by distillation over Na/benzophenone. Dichloromethane and dimethylformamide (DMF) were dried by distillation over CaH_2 . Thin-layer chromatography using silica gel 60 A° F-254 plates was used to monitor the progress of reactions. The plates were visualized first by UV illumination and then by staining using a p-anisaldehyde stain. Column chromatography was performed using silica gel (230–400 mesh).

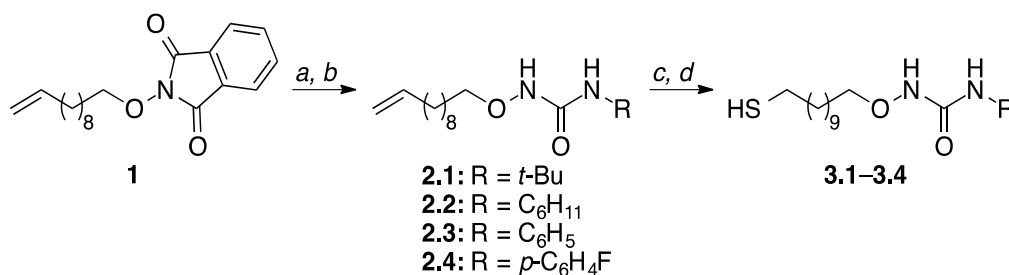
2.2. Thiol Ligand Syntheses

Syntheses of the three series of thiol-urea ligands with the general structure I, II and III in Table 1 were accomplished according to Schemes 1–3 using routes analogous to the reported synthesis of 1-(tert-butyl)-3-((11-mercapto-undecyl)oxy)urea (3.1, Scheme 1) [36]. Step-by-step procedures for the synthesis of all ligands as well as all compound characterizations are provided in the Supporting

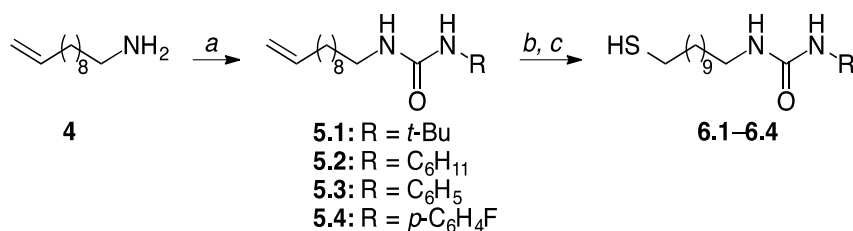
Information (SI). All intermediate compounds and the final thiol ligands were analyzed and confirmed by ^1H and ^{13}C NMR spectroscopy. Exact masses of these compounds were obtained on a hybrid linear ion trap (LIT) FT-ICR mass spectrometer.

Table 1. Panel of thiol-urea ligands synthesized for comparison.

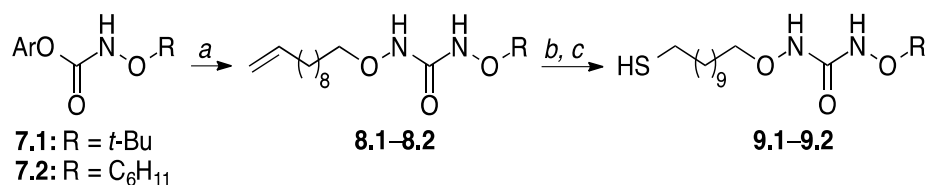
Series I Alkoxy Alkyl (3.1–3.4)	Series II Dialkyl (6.1–6.4)	Series III Dialkoxy (9.1–9.2)



Scheme 1. Synthesis of N-alkoxy-N'-alkylurea thiols 3.1–3.4 (Series I). Reagents and conditions: a. H_2NNH_2 , THF, CH_2Cl_2 , 0°C to r.t.; b. R-NCO , Et_3N , CH_2Cl_2 , 0°C to r.t.; c. $\text{CH}_3\text{C}(\text{O})\text{SH}$, cat. AIBN, THF, reflux; d. HCl , EtOH , reflux. AIBN = azoisobutyronitrile.



Scheme 2. Synthesis of N,N'-dialkylurea thiols 6.1–6.4 (Series II). Reagents and conditions: a. R-NCO , Et_3N , CH_2Cl_2 , 0°C to r.t.; b. $\text{CH}_3\text{C}(\text{O})\text{SH}$, cat. AIBN, THF, reflux; c. HCl , EtOH , reflux.



Scheme 3. Synthesis of N,N'-dialkoxyurea thiols 9.1–9.2 (Series III). Reagents and conditions: a. $\text{H}_2\text{C}=\text{CH}(\text{CH}_2)_9\text{ONH}_2$ (fr. 1), Et_3N , CH_2Cl_2 , 0°C to r.t.; b. $\text{CH}_3\text{C}(\text{O})\text{SH}$, cat. AIBN, THF, reflux; c. HCl , EtOH , reflux. Ar = *p*- $\text{C}_6\text{H}_4\text{NO}_2$.

2.3. Thiol-Functionalized AuNP Synthesis

The Series I-III thiol-urea ligands in Table 1 were used as capping agents in the two-phase reduction approach developed by Brust et al. [41] to yield monolayer-protected gold nanoparticles that then were purified by precipitation from ethanol. A brief description of the method is presented here and follows the synthesis of 1-(tert-butyl)-3-(11-mercaptoundecyl)urea-functionalized AuNPs [36]. A solution containing HAuCl_4 (0.05 g) dissolved in deionized water (4 mL) and another solution containing TOAB (0.08 g) in toluene (920 mL) were prepared. The HAuCl_4 solution was then added into the solution of TOAB with vigorous stirring until all the HAuCl_4 solution had transferred into the toluene solution. Each thiol of the three Series in Table 1 at a thiol: Au molar ratio of 1:1 was then added to the reaction mixture. Then, a freshly prepared aqueous solution of NaBH_4 (0.056 g) in deionized water (4 mL) was slowly added to the mixture with vigorous stirring. There was a rapid color change on NaBH_4 addition. After reaction, the organic phase was separated and the AuNPs were precipitated by dropwise addition of the organic phase into ethanol (400 mL) with rapid stirring. The average diameter of the thiol-coated AuNPs prepared in this way was about 2 nm as obtained from transmission electron microscopy images [36].

2.4. Fabrication of Interdigitated Electrodes and Thiol-Coated AuNP Chemiresistors

The detailed process of the fabrication of platinum interdigitated electrodes (IDE) has been reported [36]. The fabrication of thiol-coated AuNP sensors is briefly described here. AuNPs functionalized by all thiol ureas in Table 1 were dispersed in toluene (0.2% *w/w*) by sonication at ambient temperature. Then, the AuNPs dispersions were dropwise cast onto the platinum IDE area. Roughly circular films of thiol-functionalized AuNPs with a thickness of about 200 nm were formed after evaporation of toluene at ambient temperature. The resultant films were dried overnight at 40 °C in a vacuum oven. After the film preparation, the sensors of AuNPs coated with the three series of thiol-urea ligands were characterized for sensing target analytes in air to compare sensitivity and selectivity.

2.5. Sensor Measurements

All AuNP sensors functionalized with the Series I-III thiol-urea ligands for sensing target analytes were measured in the same way for direct comparison of the responses in order to understand the effect of thiol-urea molecular structure on sensing properties. The sensors were placed inside a stainless steel test chamber with a total volume of about 300 mL. The chamber was initially evacuated and VOC samples with known concentrations of analytes were introduced from a sample bag connected to the chamber. The pressure inside the chamber increased to the atmospheric pressure within a few seconds after the VOC sample entered into the chamber. During the sensing measurement, there was no air flow through the test chamber and the pressure inside the chamber was the atmospheric pressure. After testing the sample for a fixed time (e.g., 5 min), the chamber was evacuated for the next cycle of measurement.

VOC samples were prepared using Tedlar bags that had been washed with synthetic air three times. A calculated amount analyte was injected into a Tedlar bag containing 1L synthetic air for a given concentration. The concentrations of acetone in synthetic air samples were verified by a microreactor capture method as previously reported [42]. The sensors responded to VOCs with different concentrations in synthetic air by changing the resistance of the thiol-functionalized AuNP thin films on the IDE. The resistance was measured at an applied voltage using a Keithley 2400 I-V meter. All resistance data were recorded as a function of time using the Labview program. The voltage was fixed at 5 V and the current through the sensor was measured every second for calculation of the film resistance by Ohm's law. All sensor resistances were first measured over 5 min in a vacuum of 28 inch Hg below atmospheric pressure, followed by VOC sample exposure at atmospheric pressure for 5 min, and then evacuation of the testing chamber. This measurement cycle of the sensor resistance in vacuum and VOC sample exposure was repeated at least three times for all samples. Three sensors

of each thiol-functionalized AuNPs were tested for all acetone concentrations in synthetic air samples. Each sensor was examined from 10 ppb to 10 ppm of acetone in synthetic air. The responses are given as the average values of three different sensors.

3. Results and Discussion

Figure 1 shows a typical optical microscope picture of the microfabricated IDE. All IDE have the same area of $400\ \mu\text{m} \times 400\ \mu\text{m}$ and both the width of the electrodes and spaces between electrodes are $10\ \mu\text{m}$. The electrodes were made by sputtering 10-nm-thick titanium as an adhesion layer on a silicon dioxide insulating layer and a platinum layer (200 nm thick) on the top of the titanium layer. Thiol-functionalized AuNPs dispersed in toluene were droplet cast on the IDE to form sensors.

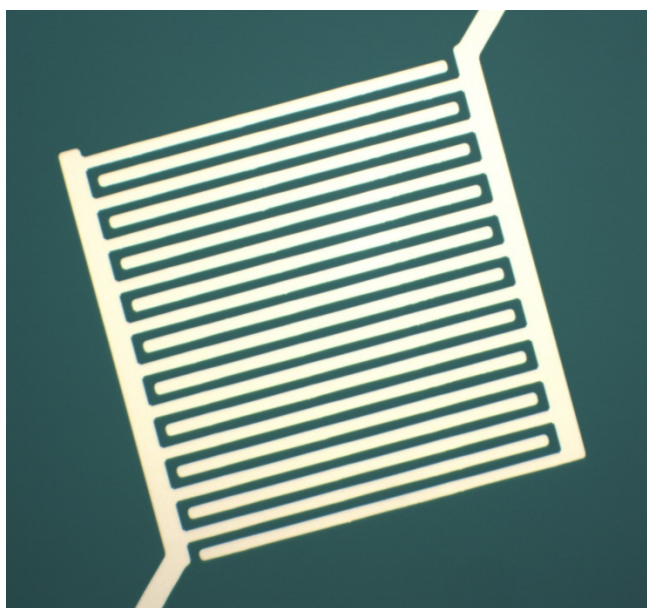


Figure 1. Microfabricated Pt/Ti platinum interdigitated electrodes (IDE) with $10\ \mu\text{m}$ of both the width of the electrodes and the space between electrodes.

The AuNP sensors derived from Series I (3.1–3.4), Series II (6.1–6.4), and Series III (9.1–9.2) shown in Table 1 were compared for sensing acetone in synthetic air. The resistance of all sensors decreased for acetone in synthetic air in comparison with the resistance in synthetic air. Therefore, the sensor response to acetone in synthetic air is defined by the following equation according to the literature for sensing target analytes with decreased resistance [15,16]:

$$\text{Response} = (R_o - R_{\text{gas}})/R_{\text{gas}} \quad (1)$$

where R_o and R_{gas} are the resistances of the sensor in synthetic air and in the presence of the acetone samples, respectively.

Figure 2 shows typical responses of the AuNP sensors derived from the three *t*-butyl analogs (3.1, 6.1, 9.1) over a wide concentration range of acetone, from 10 ppb to 10 ppm in synthetic air. For all tested concentrations, the AuNP sensors were sensitive toward acetone concentrations when coated with the alkoxy alkyl (Series I) thiol-urea 3.1 (Figure 2A) and dialkyl (Series II) thiol-urea 6.1 (Figure 2B), but not sensitive when using the dialkoxy (Series III) thiol-urea 9.1 (Figure 2C). The Series II *t*-butyl analog exhibited the highest response for all acetone concentrations that were studied. The *N*-alkyl-*N'*-*t*-butylurea-functionalized AuNPs sensor has both the highest sensitivity and lowest detection limit. Thus, the dialkyl thiol-urea 6.1 functionalized AuNP sensor provides higher responses than the alkoxy alkyl urea 3.1 and bisalkoxy urea 9.1 functionalized AuNP sensor.

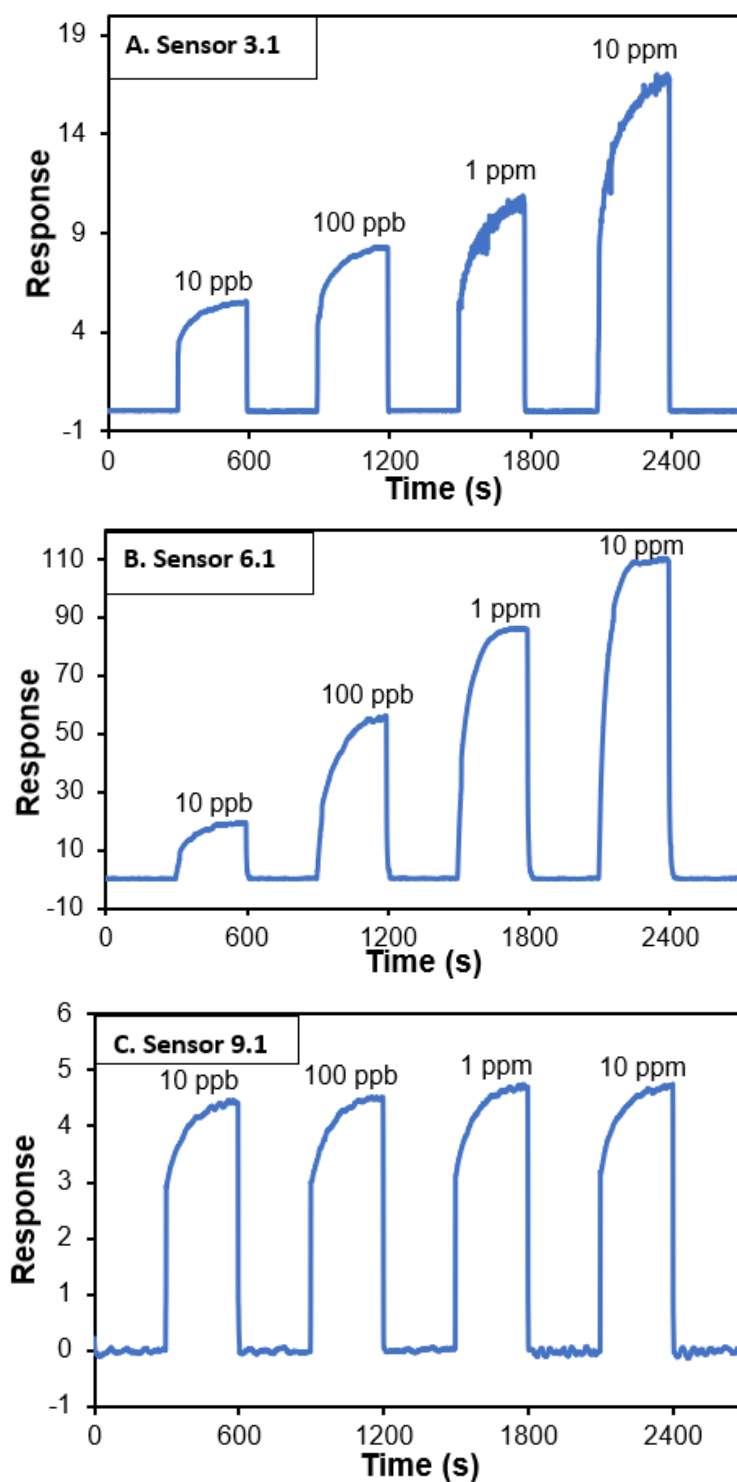


Figure 2. Responses of gold nanoparticle (AuNP) sensors derived from (A) N-alkoxy-N'-t-butyl urea 3.1, (B) N-alkyl-N'-t-butyl urea 6.1, and (C) N-alkoxy-N'-t-butoxy urea 9.1 for sensing acetone from 10 ppb to 10 ppm.

To understand steric effects of the thiol-urea ligands and interactions between urea and the target analyte, we tested the response of AuNP sensors derived from all 10 thiol-ureas (Table 1) for sensing acetone (Figure 3). The inset of Figure 3 depicts a magnified view of the sensor responses below 6. We ascribe the larger responses observed for the t-butyl-substituted thiol-urea sensors (3.1, 6.1, 9.1), relative to the other peripherally substituted sensors within a given series, to a steric effect as well

as coupled electronic interactions. We postulate that the bulkier t-butyl group decreases the ability to form H-bonds between adjacent thiol-urea ligands due to increased steric interactions [43,44]. This prevents close self-assembly of the ligands on the AuNP surfaces, which consequently increases opportunities for H-bonding with acetone. The peripheral cyclohexyl, phenyl and fluorophenyl groups of the dialkyl urea and mono-alkoxy alkyl urea ligands, Series I and II, respectively, did not provide high responses and sensitivity. These results point toward controlling the extent of the H-bonding network between urea moieties so as to enable interactions with carbonyl analytes. In this instance, the t-butyl substituent is sufficiently bulky to disrupt H-bonding between thiol-urea ligands on the AuNP surfaces to afford acetone access the urea group of the thiol to form H-bonding as illustrated Figure 4. Indeed, the effects of peripheral end groups of thiol amides on self-assembly at the surface of AuNPs have been studied by solid-state infrared spectroscopy and the results indicated that t-butyl groups have a weak H-bonding network, whereas aromatic end groups enhance H-bonding through favorable π -stacking interactions [37]. The near planar conformations of the cyclohexyl group presumably do not provide a sufficient steric barrier to disrupt the ligand H-bonding network.

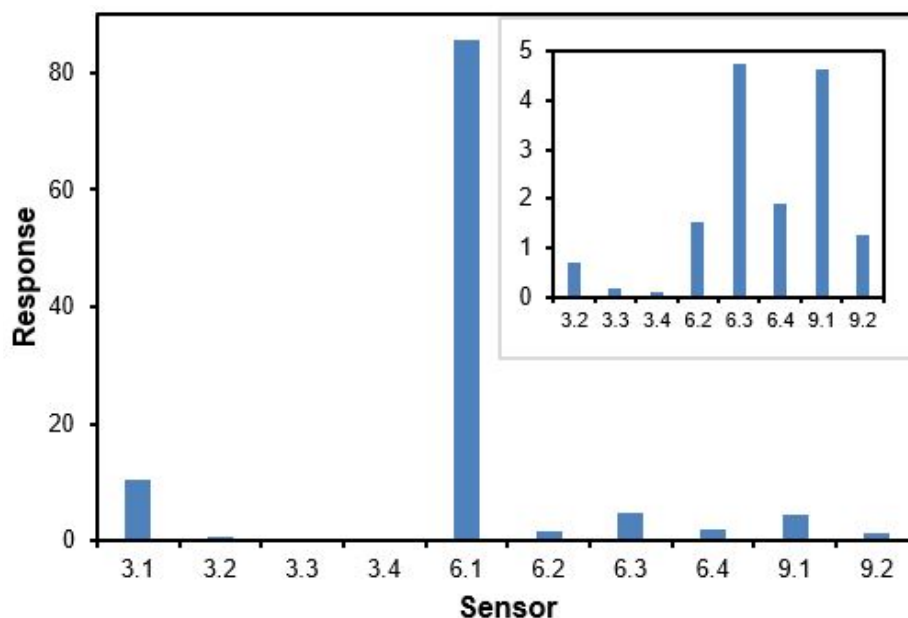


Figure 3. Response patterns for ten sensors functionalized with thiol-ureas (3.1–3.4 of Series I, 6.1–6.4 of Series II and 9.1–9.2 of Series III) listed in Table 1 for sensing 1 ppm acetone in synthetic air. The inserted graph is a magnified view of all responses below 6.

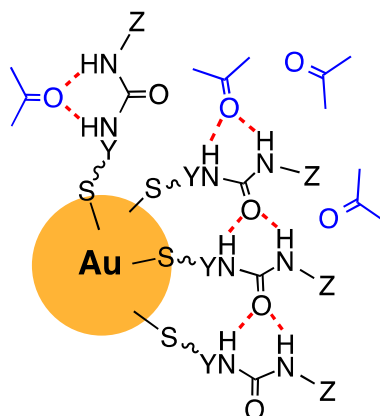


Figure 4. Model of H-bonding interactions between thiol-urea ligands (Series I, Y = O; II, Y = CH₂; III, Y = O) and acetone at the surface of AuNPs where Z = peripheral alkyl, aryl, or alkoxy group.

By comparing the responses of ligands from different Series that have the same peripheral groups (Figure 4, Z = *t*-butyl, cyclohexyl, phenyl and fluorophenyl), it is clear that the dialkyl urea functionality (Series II) affords sensors (Figure 3, sensors e-h) that exhibit higher responses than the corresponding sensors derived from ligands having alkoxy alkyl urea or bisalkoxy urea functionality. The higher responses for the dialkyl urea-based sensors may be explained in part by the absence of an α -effect (i.e., the presence of an electronegative atom adjacent to the urea NH) [45,46]. The presence of the adjacent oxygen in the Series I and III ligands influences the urea NH acidity. Considering the relative pKa's of protonated aminoxy (RONH_3^+ , 5) [47] vs. aminium (RNH_3^+ , 10), it is reasonable to expect that both the alkoxy alkyl urea and dialkyl urea will be more acidic than the dialkyl urea [48]. Higher urea acidity, in turn, will result in a more extensive H-bonding network between adjacent urea ligands. As intermolecular forces contribute to pack the ligand chains closer together, it becomes more difficult for carbonyl analytes to H-bond with the urea moiety and become associated with the AuNP surface. Thus, the weaker H-bonding network of the dialkyl urea motif and the steric destabilization afforded by the *t*-butyl end group, as in the sensor derived from ligand 6.1 in Scheme 2, combine to provide the highest sensor response for detection of acetone.

Given the high response toward acetone when using the *t*-butyl substituted dialkyl urea 6.1, we further compared the acetone-sensing sensitivity and selectivity of this thiol urea functionalized AuNP sensor with its responses to ethanol, water and benzene. Figure 5 shows that the smaller slopes of the sensor response obtained for ethanol (0.39), water (0.35) and benzene (2.52) compared to that of acetone (33.2). The slope of the sensor's linear response to the log function of the analytes is a direct measure of the sensitivity and selectivity. The results indicate that the sensor has much higher sensitivity and selectivity for acetone than ethanol, water and benzene. The response of the sensor to acetone is about 20 times of that to ethanol and water and seven times of that to benzene at the concentration of 1 ppm in synthetic air. The H-bonding-induced association of acetone with the urea group of the *t*-butyl substituted dialkyl urea 6.1 increased the sensitivity and selectivity of the sensor.

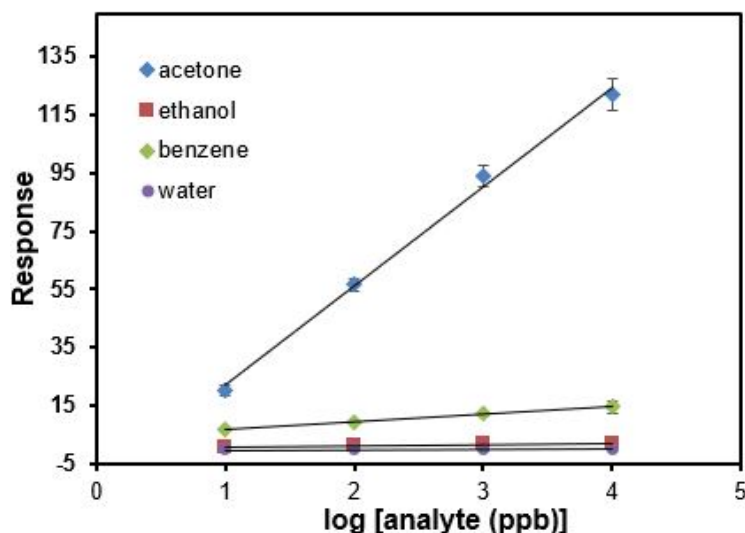


Figure 5. Response of a AuNP sensor derived from *t*-butyl urea 6.1 vs. $\log[\text{analyte (ppb)}]$ in the detection of acetone, ethanol and benzene.

4. Conclusions

Thiol-urea ligand panels featuring alkoxy alkyl, dialkyl, and dialkoxo urea groups having different peripheral substituents were synthesized to examine the effect of molecular structures on gold nanoparticle-based gas sensing properties. The dialkyl urea-functionalized AuNP sensors (Series II) showed the higher sensitivities, among which the ligand having a *t*-butyl end group exhibited the highest sensitivity as well as selectivity toward detecting acetone. The results suggest that modulation

of the intermolecular H-bonding network between ligand chains, a function of urea acidity and end group destabilization, is an important means for improving the sensitivity and possibly selectivity. The results also support the concept of using designed thiols for selective interaction with target analytes based on functional group interactions, such as urea-carbonyl H-bonding, to furnish chemoselective AuNP chemiresistors with enhanced sensitivity.

Supplementary Materials: The following Materials and Analytical Methods, thiol synthesis procedures and ^1H and ^{13}C NMR Spectra are available online at <http://www.mdpi.com/1424-8220/20/24/7024/s1>.

Author Contributions: Author Contributions: Conceptualization, X.-A.F. and M.H.N.; methodology, Z.X., M.V.R.R. and P.K.A.; thiol synthesis: M.V.R.R. and P.K.A.; sensor measurements: Z.X.; writing—original draft preparation, Z.X. and M.V.R.R.; writing—review and editing, X.-A.F. and M.H.N.; funding acquisition, X.F. and M.H.N. All authors have read and agreed to the published version of the manuscript.

Funding: This research was funded by NIH grant number: P42 ES023716.

Conflicts of Interest: The authors declare no conflict of interest. The funders had no role in the design of the study; in the collection, analyses, or interpretation of data; in the writing of the manuscript, or in the decision to publish the results.

References

1. Li, P.; Xia, H.; Dai, Y.Z.; Yang, H.; Liu, T. Microsensor based on gold nanoparticles for fast and sensitive ortho-xylene detection. *IEEE Sens. J.* **2020**, *20*, 12552–12557. [[CrossRef](#)]
2. Tang, C.; Ku, K.H.; Luo, S.X.; Concellon, A.; Wu, Y.C.; Lu, R.Q.; Swager, T.M. Chelating phosphine ligand stabilized AuNPs in methane detection. *ACS Nano* **2020**, *14*, 11605–11612. [[CrossRef](#)] [[PubMed](#)]
3. Ibañez, F.J.; Zamborini, F.P. Chemiresistive sensing with chemically modified metal and alloy nanoparticles. *Small* **2012**, *8*, 174–202. [[CrossRef](#)] [[PubMed](#)]
4. Zhou, W.; Gao, X.; Liu, D.; Chen, X. Gold nanoparticles for in vitro diagnostics. *Chem. Rev.* **2015**, *115*, 10575–10636. [[CrossRef](#)] [[PubMed](#)]
5. Saha, K.; Agasti, S.; Kim, C.; Li, X.; Rotello, V. Gold nanoparticles in chemical and biological sensing. *Chem. Rev.* **2012**, *112*, 2739–2779. [[CrossRef](#)]
6. Wohltjen, H.; Snow, A.W. Colloidal metal-insulator-metal ensemble chemiresistor sensor. *Anal. Chem.* **1998**, *70*, 2856–2859. [[CrossRef](#)]
7. Nakhleh, M.K.; Amal, H.; Jeries, R.; Broza, Y.Y.; Aboud, M.; Peled, N.; Haick, H. Diagnosis and classification of 17 diseases from 1404 subjects via pattern analysis of exhaled molecules. *ACS Nano* **2017**, *11*, 112–125. [[CrossRef](#)]
8. Grzelczak, M.; Liz-Marzan, L.; Klajn, R. Stimuli-response self-assembly of nanoparticles. *Chem. Soc. Rev.* **2019**, *48*, 1342–1361. [[CrossRef](#)]
9. Kareem, H.; Shan, S.; Wu, Z.P.; Velasco, L.; Moseman, K.; O'Brien, C.; Tran, D.T.; Lee, I.C.; Maswadeh, Y.; Yang, L.; et al. Catalytic oxidation of propane over palladium alloyed with gold: An assessment of the chemical and intermediate species. *Catal. Sci. Technol.* **2018**, *8*, 6228–6240.
10. Sibakoti, T.R.; Jasinski, J.B.; Nantz, M.H.; Zamborini, F.P. Iodine activation: A general method for catalytic enhancement of thiolate monolayer-protected metal clusters. *Nanoscale* **2020**, *12*, 12027–12037. [[CrossRef](#)]
11. Dreaden, E.C.; Alkilany, A.M.; Huang, X.; Murphy, C.J.; El-Sayed, M.A. The golden age: Gold nanoparticles for biomedicine. *Chem. Soc. Rev.* **2012**, *41*, 2740–2779. [[CrossRef](#)] [[PubMed](#)]
12. Li, Z.; Askim, J.R.; Suslick, K.S. The optoelectronic nose: Colorimetric and fluorometric sensor arrays. *Chem. Rev.* **2019**, *119*, 231–292. [[CrossRef](#)] [[PubMed](#)]
13. Kassem, O.; Saadaoui, M.; Rieu, M.; Viricelle, J.P. A novel approach to a fully inkjet printed SnO₂-based gas sensor on a flexible foil. *J. Mater. Chem. C* **2019**, *7*, 12343–12353. [[CrossRef](#)]
14. Wang, Y.; Wei, Z.; Li, P.; Li, G.; Lian, K.; Zhang, W.; Zhuiykov, S.; Hu, J. Pr₆O₁₁-functionalized SnO₂ flower-like architectures for highly efficient, stable, and selective acetone detection. *IEEE Sens. J.* **2018**, *18*, 933–940. [[CrossRef](#)]
15. Güntner, A.T.; Koren, V.; Chikkadi, K.; Righettoni, M.; Pratsinis, S.E. E-nose sensing of low-ppb formaldehyde in gas mixtures at high relative humidity for breath screening of lung cancer? *ACS Sens.* **2016**, *1*, 528–535. [[CrossRef](#)]

16. Choi, K.J.; Jang, H.W. One-dimensional oxide nanostructures as gas-sensing materials: Review and issues. *Sensors* **2010**, *10*, 4083–4099. [[CrossRef](#)]
17. Comini, E. Metal oxide nanowire chemical sensors: Innovation and quality of life. *Mater. Today* **2016**, *19*, 559–567. [[CrossRef](#)]
18. Bhowmik, B.; Manjuladevi, V.; Gupta, R.K.; Bhattacharyya, P. Highly selective low-temperature acetone sensor based on hierarchical 3-D TiO₂ nanoflowers. *IEEE Sens. J.* **2016**, *16*, 3488–3495. [[CrossRef](#)]
19. Rella, R.; Spadavecchia, J.; Manera, M.G.; Capone, S.; Taurino, A.; Martino, M.; Caricato, A.P.; Tunno, T. Acetone and ethanol solid-state gas sensors based on TiO₂ nanoparticles thin film deposited by matrix assisted pulsed laser evaporation. *Sens. Actuators B* **2007**, *127*, 426–431. [[CrossRef](#)]
20. Park, J.; Shen, X.; Wang, G. Solvothermal synthesis and gas-sensing performance of Co₃O₄ hollow nanospheres. *Sens. Actuators B* **2009**, *136*, 494–498. [[CrossRef](#)]
21. Snow, E.S.; Perkins, F.K.; Robinson, J.A. Chemical vapor detection using single-walled carbon nanotubes. *Chem. Soc. Rev.* **2006**, *35*, 790–798. [[CrossRef](#)] [[PubMed](#)]
22. Llobet, E. Gas sensors using carbon nanomaterials: A review. *Sens. Actuators B Chem.* **2013**, *179*, 32–45. [[CrossRef](#)]
23. Sysoev, V.V.; Button, B.K.; Wepsiec, K.; Dmitriev, S.; Kolmakov, A. Toward the nanoscopic “Electronic nose”: Hydrogen vs carbon monoxide discrimination with an array of individual metal oxide nano- and mesowire sensors. *Nano Lett.* **2006**, *6*, 1584–1588. [[CrossRef](#)]
24. Pinto, N.J.; Ramos, I.; Rojas, R.; Wang, P.C.; Johnson, A.T., Jr. Electric response of isolated electrospun polyaniline nanofibers to vapors of aliphatic alcohols. *Sens. Actuators B* **2008**, *129*, 621–627. [[CrossRef](#)]
25. Li, C.; Chartuprayoon, N.; Bosze, W.; Low, K.; Lee, K.H.; Nam, J.; Myung, N.V. Electrospun polyaniline/poly(ethylene oxide) composite nanofibers based gas sensor. *Electroanalysis* **2014**, *26*, 711–722. [[CrossRef](#)]
26. Nakhleh, M.K.; Broza, Y.Y.; Haick, H. Monolayer-capped gold nanoparticles for disease detection from breath. *Nanomedicine* **2014**, *9*, 1991–2002. [[CrossRef](#)]
27. Zhou, Y.; Khachatryan, W.; Multhoff, G.; Gao, H.L. Recent Advances in Gold Nanoformulations for Cancer Therapy. *Curr. Drug Metab.* **2018**, *19*, 768–780.
28. Ibañez, F.J.; Zamborini, F.P. Chemiresistive sensing of volatile organic compounds with films of surfactant-stabilized gold and gold-silver alloy nanoparticles. *ACS Nano* **2008**, *2*, 1543–1552. [[CrossRef](#)]
29. Peng, G.; Tisch, U.; Adams, O.; Hakim, M.; Shehada, N.; Broza, Y.Y.; Billan, S.; Abdah-Bortnyak, R.; Kuten, A.; Haick, H. Diagnosing lung cancer in exhaled breath using gold nanoparticles. *Nat. Nanotechnol.* **2009**, *4*, 669–673. [[CrossRef](#)]
30. Han, L.; Shi, X.; Wu, W.; Kirk, F.L.; Luo, J.; Wang, L.; Mott, D.; Cousineau, L.; Lim, S.I.-I.; Lu, S.; et al. Nanoparticle-structured sensing array materials and pattern recognition for VOC detection. *Sens. Actuators B* **2005**, *106*, 431–441. [[CrossRef](#)]
31. Krasteva, N.; Besnard, I.; Guse, B.G.; Bauer, R.E.; Müllen, K.; Yasuda, A.; Vossmeier, T. Self-assembled gold nanoparticle/dendrimer composite films for vapor sensing applications. *Nano Lett.* **2002**, *2*, 551–555. [[CrossRef](#)]
32. Cai, Q.-Y.; Zellers, E.T. Dual-chemiresistor GC detector employing monolayer-protected metal nanocluster interfaces. *Anal. Chem.* **2002**, *74*, 3533–3539. [[CrossRef](#)] [[PubMed](#)]
33. IOM. *Secondhand Smoke Exposure and Cardiovascular Effects*; The National Academies: Washington, DC, USA, 2010; p. 228.
34. U.S. EPA. *National Air Toxics Trends Station Work Plan Template*; U.S. Environment Protection Agency: Washington, DC, USA, 2011.
35. Kaftory, M.; Kapon, M.; Botoshansky, M. Role of hydrogen bonding in determining the crystal structures of the adducts between acetone and urea derivatives. *Chem. Mater.* **1994**, *6*, 1245–1249. [[CrossRef](#)]
36. Xie, Z.; Raju, M.V.R.; Stewart, A.C.; Nantz, M.H.; Fu, X.-A. Imparting sensitivity and selectivity to a gold nanoparticle chemiresistor through thiol monolayer functionalization for sensing acetone. *RSC Adv.* **2018**, *8*, 35618–35624. [[CrossRef](#)]
37. Paulini, R.; Frankamp, B.L.; Rotello, V.M. Effects of branched ligands on the structure and stability of monolayers on gold nanoparticles. *Langmuir* **2002**, *18*, 2368–2373. [[CrossRef](#)]
38. Park, S.; Yousaf, M.N. An interfacial oxime reaction to immobilize ligands and cells in patterns and gradients to photoactive surfaces. *Langmuir* **2008**, *24*, 6201–6207. [[CrossRef](#)]

39. Steemers, L.; Wanner, M.J.; Lutz, M.; Hiemstra, H.; van Maarseveen, J.H. Synthesis of spiro quasi[1]catenanes and quasi[1]rotaxanes via a templated backfolding strategy. *Nat. Commun.* **2017**, *8*, 15392. [[CrossRef](#)]
40. Willwacher, J.; Rakshit, S.; Glorius, F. Investigating N-methoxy-N'-aryl ureas in oxidative C-H olefination reactions: An unexpected oxidation behaviour. *Org. Biomol. Chem.* **2011**, *9*, 4736–4740. [[CrossRef](#)]
41. Brust, M.; Walker, M.; Bethell, D.; Schiffrin, D.J.; Whyman, R. Synthesis of thiol-derivatised gold nanoparticles in a two-phase liquid-liquid system. *J. Chem. Soc. Chem. Commun.* **1994**, 801–802. [[CrossRef](#)]
42. Li, M.; Biswas, S.; Nantz, M.H.; Higashi, R.M.; Fu, X.-A. Preconcentration and analysis of trace volatile carbonyl compounds. *Anal. Chem.* **2012**, *84*, 1288–1293. [[CrossRef](#)]
43. Anslyn, E.V.; Dougherty, D.A. *Modern Physical Organic Chemistry*; University Science Books: Sausalito, CA, USA, 2006; pp. 104–105.
44. Smith, M.B. *March's Advanced Organic Chemistry*, 7th ed.; John Wiley and Sons, Inc.: Hoboken, NJ, USA, 2013; pp. 182–184.
45. Grekov, A.P.; Veselov, V.Y. The α -effect in the chemistry of organic compounds. *Russ. Chem. Rev.* **1978**, *47*, 631–648. [[CrossRef](#)]
46. Edwards, J.O.; Pearson, R.G. The factors determining nucleophilic reactivities. *J. Am. Chem. Soc.* **1962**, *84*, 16–21. [[CrossRef](#)]
47. Ruiz-Chica, A.J.; Medina, M.A.; Sánchez-Jiménez, F.; Ramírez, F.J. Characterization by Raman spectroscopy of conformational changes on guanine-cytosine and adenine-thymine oligonucleotides induced by aminoxy analogues of spermidine. *J. Raman Spectrosc.* **2004**, *35*, 93–100. [[CrossRef](#)]
48. Bordwell, F.G.; Ji, G.Z. Effects of structural changes on acidities and homolytic bond dissociation energies of the H-N bonds in amidines, carboxamides, and thiocarboxamides. *J. Am. Chem. Soc.* **1991**, *113*, 8398–8401. [[CrossRef](#)]

Publisher's Note: MDPI stays neutral with regard to jurisdictional claims in published maps and institutional affiliations.



© 2020 by the authors. Licensee MDPI, Basel, Switzerland. This article is an open access article distributed under the terms and conditions of the Creative Commons Attribution (CC BY) license (<http://creativecommons.org/licenses/by/4.0/>).